Journal of Shanghai University (*English Edition*), 2007, **11**(1): 1–16
Digital Object Identifier(DOI): 10.1007/s 11741-007-0101-6

· ***Review*** ·

Reliability aspects of electronics packaging technology using anisotropic conductive adhesives

LIU Johan (刘建影)[1,2], LU Xiu-zhen (路秀真)[1], CAO Li-qiang (曹立强)[2]
1. Key State Lab of Advanced Displays and System Integration and SMIT Center, Shanghai University, Shanghai 200072, P. R. China
2. SMIT Center, Department of Microtechnology and Nanosciences, Chalmers University of Technology, SE-412 96 Göteborg, Sweden

Abstract Anisotropic conductive adhesive technology for electronics packaging and interconnect application has significantly been developed during the last few years. It is time to make a summary of what has been done in this field. The present paper reviews the technology development, especially from the reliability point of view. It is pointed out that anisotropic conductive adhesives are now widely used in many applications and the reliability data and models have been developed to a large extent for anisotropic conductive adhesives in various applications.

Keywords electronics packaging, anisotropic conductive adhesives, reliability.

1 Introduction to anisotropic conductive adhesive technology

Recent environmental legislation has led to an increasing interest in the possibility of substituting electrically conductive adhesives for the traditional tin-lead solders in electronics manufacturing. The conductive adhesives mentioned in this chapter are composites of insulating polymer matrix and conductive fillers. Depending on the loading of fillers, conductive adhesives can be cataloged as isotropic conductive adhesive (ICA) and anisotropic conductive adhesive (ACA). In this paper, our topic focuses on the ACA. ACA is a new class of adhesives that are conductive in one direction, which offers the following advantages over traditional tin-lead solders in the interconnections[1].

- Low temperature processing.
- Compatibility with a wide range of substrates.
- No flux pretreatment or post-cleaning procedures required.
- No lead or other toxic metals.
- Finer pitch capability.
- Solder mask not required.

ACAs are prepared by dispersing conductive fillers in an adhesive matrix. The unidirectional conduction is achieved by using a relatively low volume fraction of conductive fillers. This low filler loading is insufficient for inter-particle contact and prevents conduction in the $X-Y$ plane of the adhesive, but enough particles are present to assure reliable conduction between bonding electrodes in the Z direction[2]. Because of the anisotropy, ACAs can be deposited over the entire contact region, greatly expanding the bonding area. Also the low filler loading improves the bonding strength. Thus mechanically robust interconnection can be achieved with ACA assembly.

ACAs come in two distinct forms: paste and film. Pastes can be printed with screen or stencil, or dispensed with a syringe. Films are supplied by manufacturers as reel and extremely suitable for non-planar bonding surfaces. Both thermoplastic and thermosetting resins have been used as adhesive matrices. The principal advantage of thermoplastic ACAs is the relative ease to disassemble the interconnections for repair operation, while thermosetting adhesives possess higher strength at elevated temperature and form more robust bonds[2]. The commonly used conductive fillers include silver and nickel particles and polymer spheres coated with metal (Ni/Au). Silver particles offer moderate cost, high electrical conductivity and low chemical reactivity. Nickel particles can break the oxide layer on the electrodes and are suitable for interconnecting easily oxidized metal. Metal-coated polymer spheres have fairly uniform diameter distributions. They can provide high interconnection reliability because of the large elastic deformation during bonding. Recent application of solder particles as ACA fillers has also been reported[3].

Since the conduction of ACAs is based on mechanical particle-electrode contacts, pressure is a requisite to

Received Sep.25, 2006
Corresponding author LIU Johan, PhD, Prof., E-mail: johan.liu@mc2.chalmers.se

form qualified joints. A typical ACA assembly is shown in Fig.1. After alignment, pressure is applied on the backside of the chip. The adhesive resin is squeezed out and conductive particles are trapped and deformed between opposing electrodes. Once electrical continuity is generated, the adhesive resin is cured with heat or UV. The intimate particle-electrode contacts are maintained by the cured matrix and the elastic deformation of particles and electrodes exerts a continuous contact pressure.

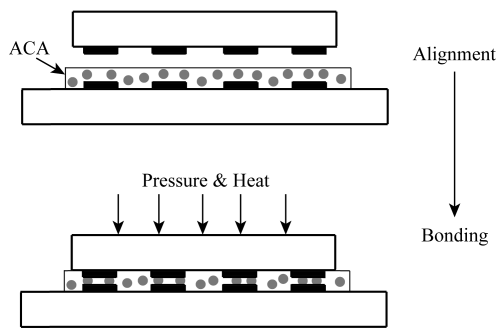

Fig.1 Manufacturing process of ACA assembly

ACA interconnection finds particular applications with fine-pitched flip-chip techniques used to mount bare chip on various substrates such as ITO coated glass, FR-4 board and flexible films[4]. ACA joining is also attractive for fine-pitched surface mount component assembly. However, the performance and reliability of ACA joints are more sensitive to the joint design, substrate/component properties and process conditions than solder joints. In Section 2, some important parameters are addressed and their effects on joint reliability are described.

2 Reliability of ACA interconnects

2.1 Experimental evaluation

With regard to the reliability of conductive adhesive joints, contact resistance of single joints is the most important feature. Liu and Lai[5] investigated the reliability performance of ACA flip-chip joints on FR-4 boards. In the study, nine types of ACAs (A-I) and one pure adhesive without any particles (J) were evaluated and some relevant technical data are shown in Table 1. As shown in Fig.2, the test chip had a pitch of 100 μm, containing 18 single joints and two daisy-chains (18 joints for each). The substrate used was a 0.8 mm thick FR-4 rigid board. Therefore, the work was particularly focused on the reliability of ultra fine pitch ACA flip-chip interconnects on low-cost substrates. In total, 954 joints (53 chips) with various ACAs were subjected to temperature cycling between −40 ℃ and 125 ℃ with a dwell time of 15 min and a ramp rate of 110 ℃/min. The contact resistance of 36 joints (two chips) with ACA A was measured *in-situ* during testing up to 3000 cycles. Other joints were taken out from the chamber every several hundreds of cycles and measured manually at room temperature.

Fig.3(a) shows a typical *in-situ* resistance change of a single joint measured at both extremes of each cycle during the test. As can be seen, the resistance increased gradually with the thermal cycles. Cumulative fails of ACA A with *in-situ* measurement are shown in Fig.3(b). The number of fails depends heavily on the definition of the failure. If the criterion was defined as 20% increase in joint resistance, all joints failed after 2000 cycles. This definition might be too harsh for those joints with only several mΩ where a 20% increase means only a few mΩ to vary. In some cases, the limitation is still within the error margin of the measurement. If an increase of 50 mΩ or 100 mΩ was used as the failure criterion, the MTTF (mean time to failure) value became 2500 and 3500 cycles, respectively. Therefore, it is very important to define suitable criteria according to the product requirements. As shown in Fig.4, the reliability data of ACA A with the various failure criteria have also been analyzed with the three-parameter Weibull distribution. In the case of 20% increase, the Weibull analysis indicated that there were always some joints that would reach this value even before the first cycle was finished

Table 1 Relevant technical data of ACAs subjected to reliability tests

Adhesive	Form	Conductive filler	Bonding condition
A	Film	Ni, 3 μm	180 ℃/10 s, 6 kg/mm^2
B	Film	Ni, 3 μm	180 ℃/10 s, 6 kg/mm^2
C	Film	Ni, 2–3 μm	160 ℃/20 s, 2.5 kg/mm^2
D	Film	Ni/Au plastic, 5 μm	160 ℃/20 s, 2.5 kg/mm^2
E	Paste	Ni/Au plastic, 3 μm	150 ℃/30 s, 5 kg/mm^2
F	Paste	Ni, 5 μm	150 ℃/30 s, 5 kg/mm^2
G	Paste	Ni/Au plastic, 5 μm	180 ℃/60 s, 7–15 kg/cm^2
H	Paste	Ni/Au plastic, 7 μm	180 ℃/60 s, 7–15 kg/cm^2
I	Paste	Ni/Au plastic, 11.5 μm	180 ℃/60 s, 7–15 kg/cm^2
J	Film	No Filler	160 ℃/20 s, 2.5 kg/mm^2

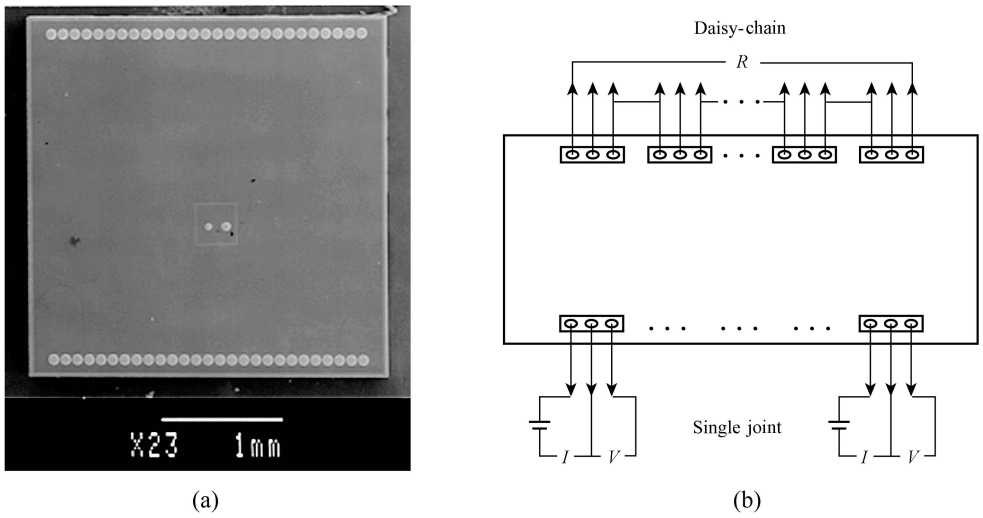

Fig.2 Test chip: (a) configuration, (b) measurement wiring of the test chip

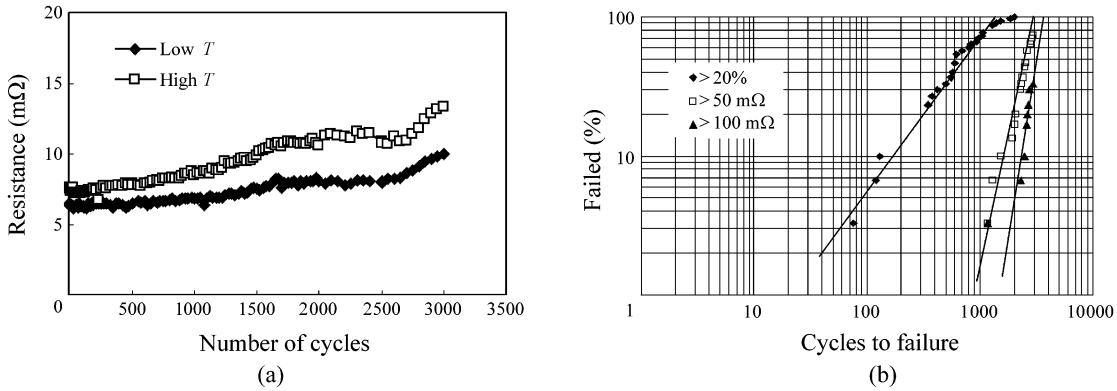

Fig.3 (a) Typical resistance evolution of a single ACA joint subjected to the temperature cycling test; (b) cumulative failures of ACA A joints during the test (Data were *in-situ* measured up to 3000 cycles)

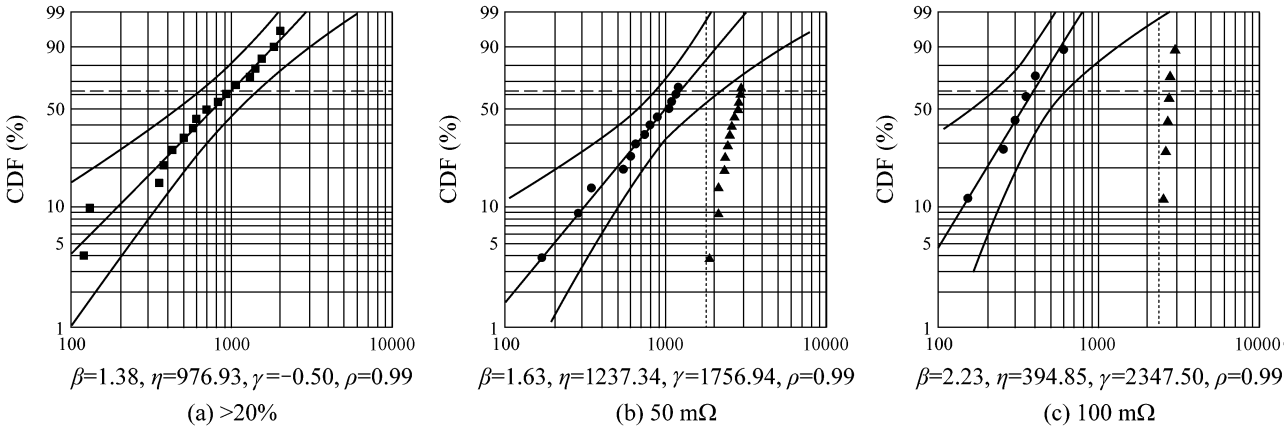

Fig.4 Weibull analyses of ACA A joints with various failure criteria: (a) >20%, (b) 50 mΩ, (c) 100 mΩ (Cycles, −40℃ to 125℃)

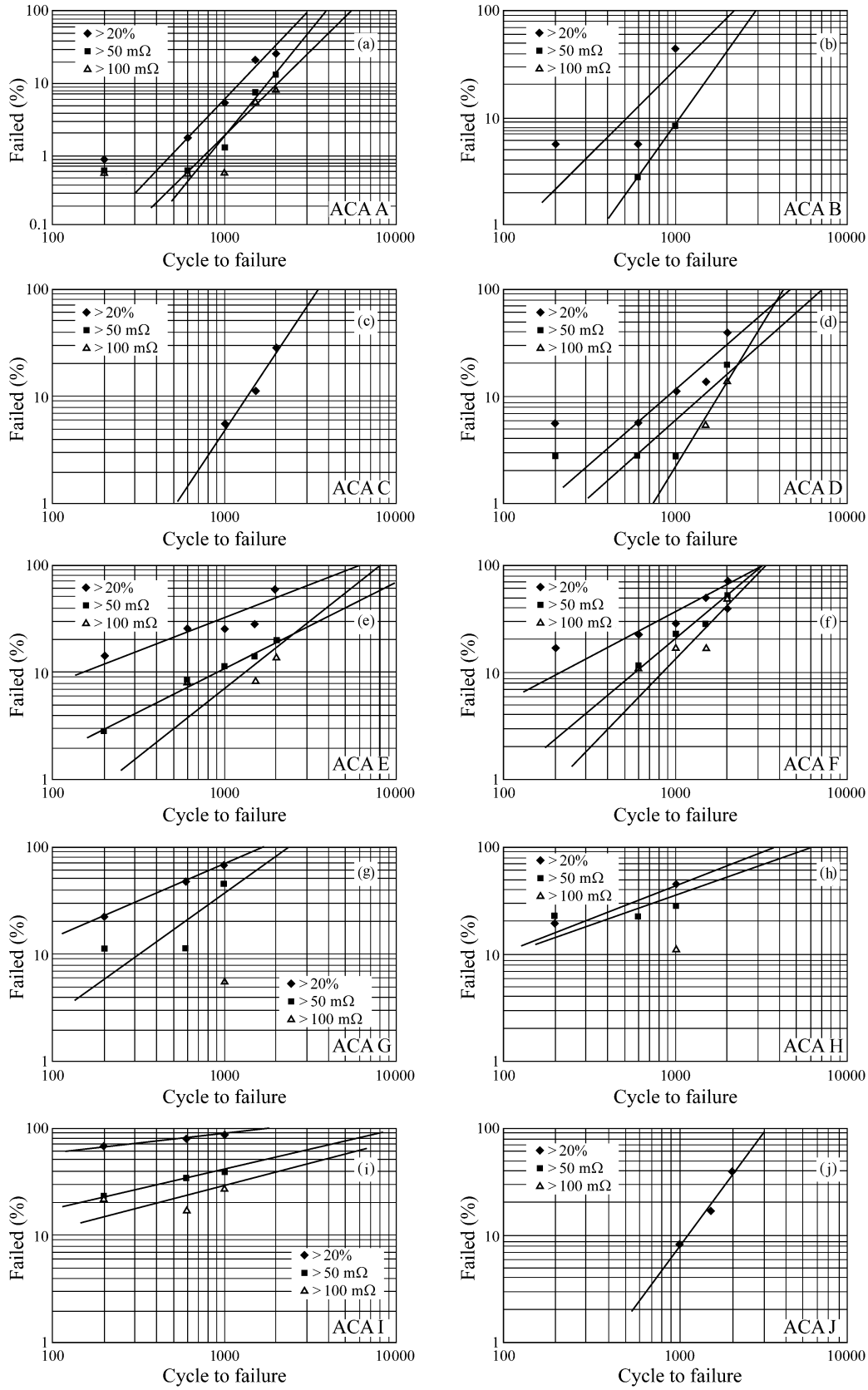

Fig.5 Cumulative failures of various ACA joints (These joints were taken out from the chamber every several hundreds of cycles and measured manually at room temperature)

($\gamma \cong 0$ in Fig.4(a)). However, if the 50 mΩ failure criterion was used, it could be guaranteed that no failure occurred within 1757 cycles (Fig.4(b)). Similarly, the first failure would occur after 2347 cycles if the 100 mΩ failure criterion was used (Fig.4(c)). In both of the latter cases, it is clear that the ACA flip-chip/FR-4 joints had quite good reliability and could withstand at least 1700 thermal cycles if an increase of 50 mΩ or higher was used as the failure criterion.

Cumulative fails of ACA joints measured manually at room temperature are shown in Fig.5. The MTTF ($>$ 20%) of joints with ACAs A, C and J was 2500 cycles. Although other joints, for example those with ACAs G, H and I, could also have a MTTF of 2500 cycles, their infant-mortality failure rate was high, which means these joints were unreliable.

If we compare the manually measured data with the *in-situ* data (Fig.3(b) and Fig.5(a)), the *in-situ* measurement gave rather pessimistic result: 50% of joints failed before 650 cycles if a 20% increase in joint resistance was used as the failure criterion. With manual measurement, the number of cycles to 50% fails was around 2500. The exact reason is not clear. However, as they are more close to the real application situations, the *in-situ* data are considered to be more important than the data measured manually at room temperature.

ACAs A and B are from the same vendor. The only difference is that ACA B uses the so-called double-layer technique to increase the fine pitch capability. As can be seen from Fig.5(a) and (b), the double-layered ACA B showed similar reliability as the single-layered ACA A. In the case 50 mΩ and 100 mΩ failure criteria were used, the MTTF of ACA B could also reach 1200 and 2200 cycles, respectively.

ACAs C and D are from another vendor. ACA C is filled with nickel particles, while ACA D is filled with nickel/gold coated plastic balls. Both of them showed good reliability performance (Fig.5(c) and (d)). Although the data scattering was large, specially in the case of ACA D, the MTTF values could reach over 2700 and 3000 cycles for the ACAs C and D, respectively.

ACAs E and F are in a paste form, different from ACAs A – D which are in a film form. As shown in Fig.5(e) and (f), their reliability was also very good. In the case of ACA E which is filled with nickel/gold coated plastic balls, the MTTF could reach 2000 cycles when the failure was defined as 20% resistance increase. If the 50 mΩ and 100 mΩ failure criteria were used, the MTTF was about 5000 cycles. ACA F, filled with nickel particles, also had a MTTF over 1500 cycles. The reliability curves in Fig.5(g)–(i) show the effect of filler size on the joint reliability. These adhesives are all filled with nickel/gold coated plastic particles. It seemed that fillers larger than 5 μm had negative effect on the joint performance. With these pastes, joints could fail rather early in the test though their MTTF values were quite high.

Fig.5(j) shows the results of joints with a pure adhesive film. It is interesting to notice that this film also showed good reliability, and the MTTF value was about 2000 cycles if the failure was defined as 50 mΩ increase. This indicates that the resin itself is extremely important in determining the reliability of the ACA joint.

2.2 Effects of assembly process

The assembly process of ACA interconnection includes alignment, bonding and, if solder interconnects exist in the same board, reflow. Due to the low surface tension, ACA interconnection lacks the benefit of the self-alignment, which put a stringent requirement on the alignment accuracy. A normal flip-chip bonder that offers a ±5 μm accuracy is normally good enough. Nevertheless, bad alignment would result from incorrect operations. It can influence the pressure distribution and, in more serious situations, decrease the contact area for electrical interconnection (Fig.6).

The bonding process is very critical to the ACA joint performance and reliability, since both mechanical integration and electrical interconnection are established in this process. Bonding pressure and temperature are two most important parameters. To achieve reliable ACA joints, adequate bonding pressure should be applied uniformly and suitable bonding temperature should be kept for sufficient time[6].

The bonding pressure is applied to force the conductive particles to contact the electrodes. The performance of the joint depends heavily on the deformation degree of particles. Ideally, the particles should be squashed enough to gain the largest contact area. However, the integration of particle body should be maintained and cracking due to over pressure could degrade the electrical performance[7].

It is also important to keep the pressure uniform during the bonding. Non-homogeneous bonding pressure can cause particles being deformed unevenly, which could result in poor long-term reliability. This problem becomes more serious for thin and flexible substrates.

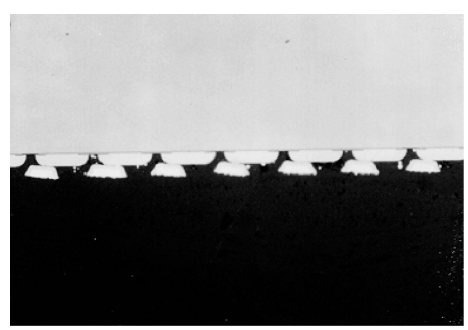

Fig.6 Bad alignment degrades the electrical performance and reliability of ACA joints

The effects of particle deformation on joint electrical reliability during temperature cycling are summarized schematically in Fig.7. Type 1 represents the best case where the particles are deformed uniformly and atomic bonding between the particles and contacts is achieved. Type 2 joints consist of un-deformed or slightly deformed particles due to either low bonding pressure or inhomogeneous pressure distribution. The conductive character of these joints is unstable at high temperature because the epoxy matrix will expand more than the particles. Type 3 joints can result from shape or height variations of the contact areas. Some particles are not deformed enough and will shrink more than those well deformed, causing problems at low temperature. Finally, Type 4 pictures a uniform height of the contact areas, but a very large variation of particle size. Due to the weak bonding between the smaller particles and contact area, electrical opens can be observed at both low and high temperatures. All these situations have been observed experimentally[6].

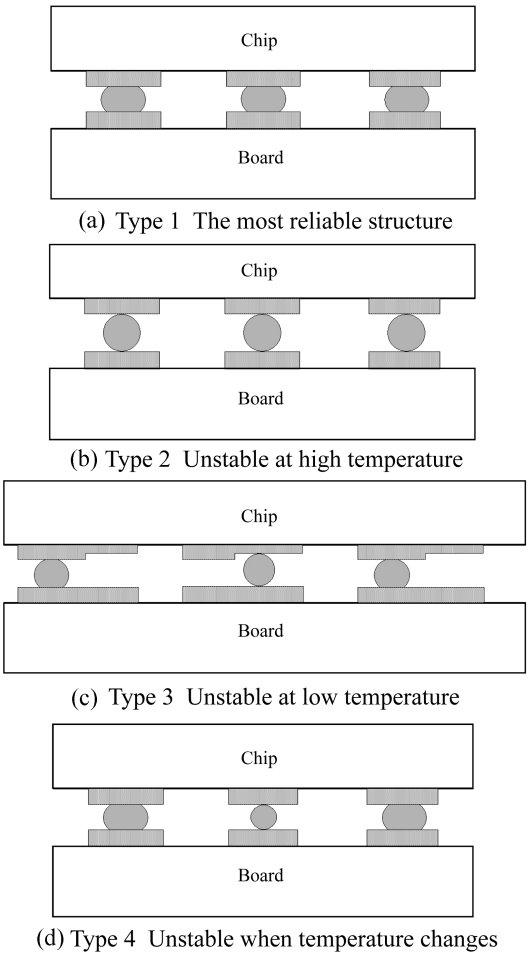

Fig.7 Schematics of four types of ACA joints caused by variations in bonding pressure, bump geometry and filler size

The bonding temperature and time heavily influence the curing degree of the adhesive that plays an important role in the reliability of ACA joints[8]. In undercured joint, the cross-linkage of the polymer may be incomplete and neither mechanical performance nor electrical reliability can be guaranteed under high humidity tests. To gain a certain curing degree, longer bonding time should be employed with lower bonding temperature. However, this is not preferable due to the low productivity. On the other hand, too high bonding temperature is not desired, either. This is because the epoxy may solidify too quickly and hence the conductive particles would not have enough time to distribute themselves in between the bumps and pads. Recent work[9] also observed the chain scission due to high bonding temperature. So finding optimum combination of bonding temperature and time is a fundamental step towards reliable ACA interconnection.

If ACA interconnection is used together with soldering technology for the final products, reflow soldering after ACA bonding is inevitable. During reflow, the package needs to be heated up to above 200℃, which is much higher than the normal bonding temperature of ACA joint. The ability of ACA interconnection to withstand this high temperature is critical for successful packaging. Yin, *et al.*[10] found that the contact resistance of ACA joints increased significantly after reflow process and conduction gaps formed between the conductive particles and the electrode. Seppälä and Ristolainen[11] also reported the detrimental effects of reflow on the reliability of ACA joints. The possible reason is that, due to its much higher coefficient of thermal expansion (CTE), the adhesive matrix expands in the Z direction much more than the particles during the reflow. The induced thermal stress lifts the chip from substrate and damages the bonding structure. Therefore, the peak temperature of reflow profile and the distance between the chip and substrate (related to bump height) are the most important factors. By optimizing process parameters and adopting ACA with lower CTE, the effects of the reflow process can be reduced to some extent[10].

2.3 Effects of substrate and component

Suitable substrate stiffness and bump dimensions are also important to achieve reliable ACA joints. With a soft substrate, significant deformation of the substrate may occur during the bonding, which has a direct influence on the joint quality[12]. On the FR-4 board it was observed that the electrical resistance and reliability of a joint depend on the distance between the pad and glass fibers in the substrate (Fig.8). A long distance means a thick layer of soft epoxy that may deform during bonding. Therefore, enough particle deformation cannot be obtained at that point. Fig.9(a) shows that large force

exerted on the pad causes the pad sinking and almost no deformation occurring in the particles. An approach to reduce the pad sinking is to use a relatively smaller bump area compared to the pad area. Therefore, less bonding force will be transferred to the pad, as shown in Fig.9(b).

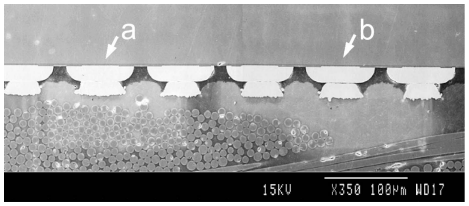

Fig.8 Electrical resistance and reliability of a joint depend on the distance between the pad and glass fibers in the substrate. Joint a has a better electrical performance than Joint b (5 mΩ *vs* 14 mΩ) due to its location closer to glass fibres

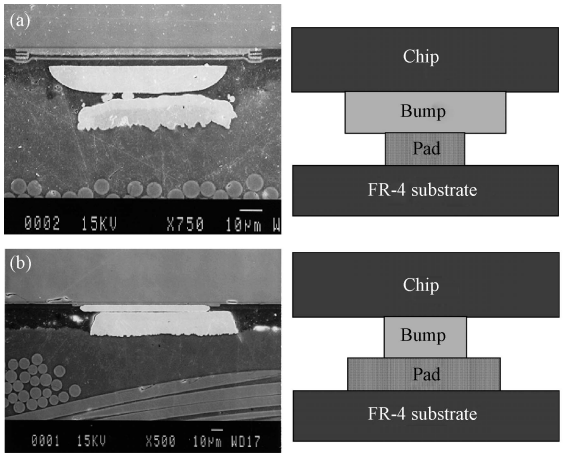

Fig.9 (a) Pad sinking leads to insufficient particle deformation; (b) using a bump smaller than the pad can decrease pad sinking

For flip-chip solder joining, plastic strain of solder bumps is a critical parameter that governs the joint reliability. Using high bump can reduce the bump strain and thus increase the joint reliability, as shown in Fig.10(a). However, a systematical study on the effect of bump height showed that the failure mechanism of ACA flip-chip joints is totally different[13]. In ACA joints, the bump and pad are usually made of metals that are much stiffer than adhesives. In other words, thermal mismatch stresses can hardly deform the bump and pad, and the shear strain is localized in the adhesive between the mating bump and pad (Fig.10(b)). In this case, the joint reliability is governed by the shear strain in the adhesive and the influence of bump height is limited. Meanwhile, the stress in the Z-axis will be raised with bump height due to the increased adhesive volume. At elevated temperature, this stress can lift the chip and weaken the joint. So benefits from high bump cannot be expected for ACA joints. Another practical problem associated with high bump is that air bubbles are easily introduced during ACA bonding.

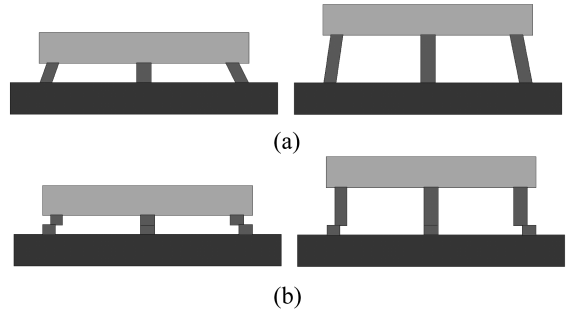

Fig.10 (a) Using high bumps can reduce the strain of solder joints; (b) it has much less influence on the strain of ACA joints

2.4 Degradation due to moisture absorption

ACAs contain a much larger quantity of polymers. Therefore, polymer degradation due to moisture absorption becomes more significant in ACA joints. Water can degrade polymers through (1) depressing of the glass transition temperature T_g and functioning as a plasticiser, (2) giving rise to swelling stresses, and (3) generating voids or promoting the catastrophic growth of voids already present. All three occurrences have been known to lead to mechanical degradation. Moisture absorption can also contribute to the disruption of conductivity in the path between mating electrodes. This may include, for example, changes in the polymer/filler dispersion state through the expansion of the polymer matrix and formation of defects like cracks and delaminations.

The effects of moisture on an ACA film was studied with Fourier transform infra-red (FTIR) spectra that provide a vast reservoir of molecular information pertaining to the chemical groups present, as well as to the structure arrangement and bonding preferences of these groups[14]. The adhesive was conditioned in two environments: 85℃/85%RH and 22℃/97%RH. After certain amount of time, samples were taken out of the chamber and FTIR spectra were collected.

Fig.11 shows, respectively, the spectra of the adhesive (a) after curing, (b) after 41 hours' exposure to 85℃/85%RH, and (c) the difference spectra representing the changes due to the moisture exposure. As shown, the negative bands at 868 cm^{-1}, 916 cm^{-1}, 1345 cm^{-1}, 3005 cm^{-1} and 3058 cm^{-1} indicate the further progress of the cure reaction. Moisture degradation is believed to occur by hydrolysis of the ester linkages, which creates two end groups, a hydroxyl and a carbonyl. Though it

is hard to see any new emerging carbonyl groups in this figure, the band at 3560 cm^{-1} indicates the existence of free hydroxyls. With more time exposure, curing effect is not observed, but degradation becomes more apparent. The spectra collected from samples exposed to 22℃/97%RH showed moisture absorption through hydrogen bonding, but neither further curing nor degradation is observed, implying the dominant degradation is associated with heat.

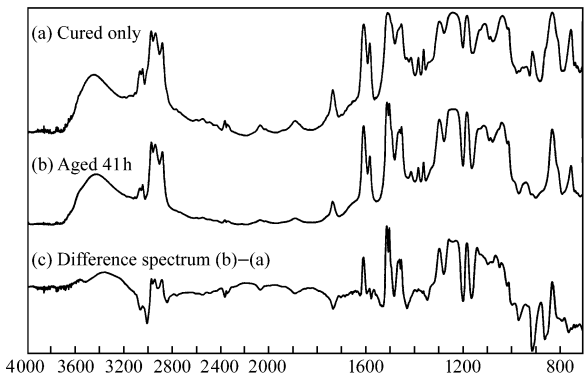

Fig.11 FTIR spectra of an ACA film (a) after curing, (b) aged at 85℃/85%RH for 41 hours, (c) the difference spectrum (b)–(a)

3 Theoretical studies and numeric simulations

3.1 Theoretical treatment of oxidation and crack growth

In order to correlate the electrical resistance shift as a function of humidity test time, a theoretical model has been developed based on [15]. It takes into account both oxidation and cracking, two primary failure mechanisms of conductive adhesive joints, and can thus explain the experimental observations quite well.

Fig.12 shows schematically the electrical conducting path through a conductive adhesive joint. Before exposure to the humid environment, the initial resistance through the joint is

$$R_{\text{init}} = R_{\text{s}} + R_{\text{j}} + R_{\text{l}}, \tag{1}$$

where R_{s} is the resistance through the substrate, R_{j} the resistance through the adhesive joint, and R_{l} the resistance through the component lead. After humidity test, the joint resistance becomes

$$R_{\text{after}} = R_{\text{s}} + R_{\text{j}} + R_{\text{l}} + R_{\text{oxide}} = R_{\text{init}} + R_{\text{oxide}}, \tag{2}$$

where R_{oxide} is the resistance through the oxide layer which can be expressed as

$$R_{\text{oxide}} = \rho_{\text{oxide}} \frac{L}{A}, \tag{3}$$

where ρ_{oxide} is the volume resistivity of the oxide layer, L the oxide layer thickness and A the contact area.

Since polymer structures normally contain a large amount of free volume, it is reasonable to assume that the diffusion of oxygen is much faster in polymers than in metal oxides. In other words, the oxygen diffusion through the oxide layer will control the oxide growth rate and consequently the increase of the resistance in the oxide layer.

Assume the following Einstein equation holds:

$$L = \sqrt{2D_{\text{oxide}}t}, \tag{4}$$

where D_{oxide} is the diffusion parameter of oxygen through the oxide layer and t is the time for the oxygen diffusion. Combining Eqs.(2)–(4), one can obtain the relationship between the time and the resistance change:

$$\frac{R_{\text{after}}}{R_{\text{init}}} = 1 + \frac{L_{\text{e}}\rho_{\text{oxide}}}{AR_{\text{init}}}\sqrt{\frac{t}{t_{\text{e}}}}, \tag{5}$$

where L_{e} is the oxide layer thickness at the end of test, t the elapsed time and t_{e} the total test time. Eq.(5) can be used to calculate the relative electrical resistance change due to oxidation.

The crack normally occurs at the interface between the adhesive and the electrode, and decreases the real contact area gradually. Here assume the contact area A can be expressed as

$$A = A_0\left(1 - \frac{t}{t_{\text{e}}}\right), \tag{6}$$

where A_0 is the original contact area. Therefore, taking into account the crack growth, the electrical resistance change becomes

$$\frac{R_{\text{after}}}{R_{\text{init}}} = 1 + \frac{L_{\text{e}}\rho_{\text{oxide}}}{A_0\left(1 - \frac{t}{t_{\text{e}}}\right)R_{\text{init}}}\sqrt{\frac{t}{t_{\text{e}}}}. \tag{7}$$

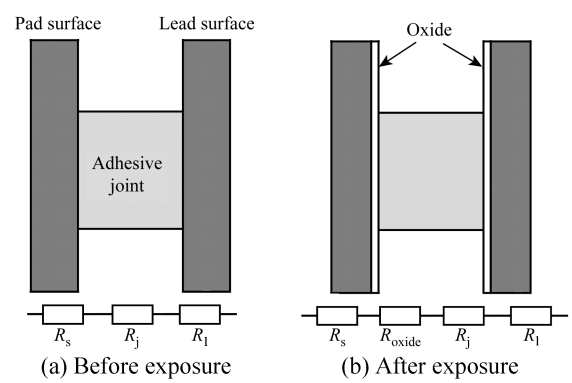

Fig.12 Electrical conducting path through a conductive adhesive joint before and after humidity exposure

Fig.13 shows the calculated results with Eqs.(5) and (7), using the parameters given in Table 2. The calculations show that if no crack is formed, the electrical resistance will increase gradually with test time, but no catastrophic failure will be expected. The effect of cracking is rather small at the beginning, but then becomes more and more significant with the increase of test time. If a complete crack forms by the end of the testing, the electrical resistance will go to infinity.

For comparison, the experimental results obtained earlier[16] are also given in Fig.13. Before 500 test hours, Eq.5 can predict the experimental observations quite well. However, the experimental results after 500 hours cannot be explained by considering the oxidation of copper metal surface only, which means that fracture must have taken place during the humidity testing. In fact, cracks have already been observed after 158 hours of exposure[16].

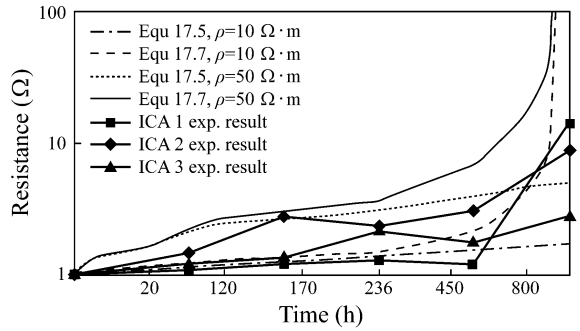

Fig.13 Calculated and observed results of electrical resistance change as a function of humidity test time for ICA joints on copper surfaces

Table 2 Parameters used for calculation of the resistance evolution of an adhesive joint at 85℃/85% RH

Bonding surface	Oxide	ρ_{oxide} ($\Omega\cdot$m)	A_0 (μm^2)	L_e (nm)	D_{oxide} (m^2/s)	$R_{\text{init}}(\Omega)$
Copper	Cu_2O	10–50	1.1×10^{-6}	20	5×10^{-20}	0.2

3.2 Process simulations of ACA interconnection

3.2.1 Probabilities of open and bridging

If the ACA contains insufficient particles, there is of course a certain probability that no particle exists in the joint and an open is resulted. On the other hand, bridging is possible due to there being too many particles in a too short spacing, causing short circuit between neighbouring pads. Accurately estimating probabilities of open and bridging is important to explore the limiting pitch of ACA interconnection at which the open/short circuit probability becomes unacceptable.

Mannan, *et al.*[17] proposed an analytical method to estimate the open probability. Assume that the number of particles on a pad obeys Poisson distribution:

$$P(n)=\frac{\mathrm{e}^{-\mu}\mu^n}{n!}, \tag{8}$$

where $P(n)$ is the probability of finding n particles on a pad and μ is the average number of particles on a pad. If the volume fraction of particles f and the particle radius r are known, μ is given by

$$\mu=\frac{3Af}{2\pi r^2}, \tag{9}$$

where A is the pad area. Thus the probability for an open ACA joint is

$$P(0)=\mathrm{e}^{-\mu}=\exp\left(-\frac{3Af}{2\pi r^2}\right). \tag{10}$$

For a typical ACA with a volume fraction of particles ranging from 3 to 15 vol% the open circuit probability on a 100 μm^2 pad varies from 10^{-13} to 10^{-3}, which is extremely small. However, in reality, there is always a crowding effect that must be taken into account. In this case, the particle distribution can be described using a binominal distribution model:

$$P(n)=C_n^N(1-s)^{N-n}s^n, \tag{11}$$

where N is the maximum number of particles that can be contained in the pad area A. C_n^N is the binominal coefficient and s is equal to f/f_m, where f_m is the volume fraction corresponding to maximum packing. In the limit that $f\ll1$, Eqs.(10)–(16) and (11)–(17) give identical results for $P(0)$.

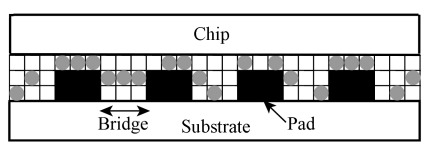

Fig.14 Schematics of bridging in the ACA interconnection (Courtesy of S.H. Mannan)

For a rough estimation of bridging, Mannan, *et al.*[18] proposed a simplified box model. As shown in Fig.14, the volume between pads can be divided into cubic boxes with sides the same length as the particle diameter. If k boxes are filled out of a total of N, the volume fraction of particles is

$$f=\frac{k\frac{4}{3}\pi r^3}{N(2r)^3}, \tag{12}$$

where r is the particle radius. Thus the probability for

a single box being occupied is given by

$$\frac{k}{N} = \frac{6f}{\pi}. \tag{13}$$

Determined by the number of boxes that can be fitted onto the side of a single pad and by $(6f/\pi)^q$ where q is the lowest number of particles needed to bridge the pad spacing, the bridging probability is given by

$$p = 1 - \left(1 - \left(\frac{6f}{\pi}\right)^{\frac{d}{4r^2}}\right)^{\frac{hl}{4r^2}}, \tag{14}$$

where h and d are the pad height and length, respectively, and l is the spacing between the pads.

This box model only gives an upper limit. Fig.15 shows the bridging probabilities derived from different models. It is clear that the lowest combined probability for bridging and skipping occurs in the volume fraction between 7% and 15%, depending on which model is used. This volume fraction range is also generally used for commercial ACA materials today.

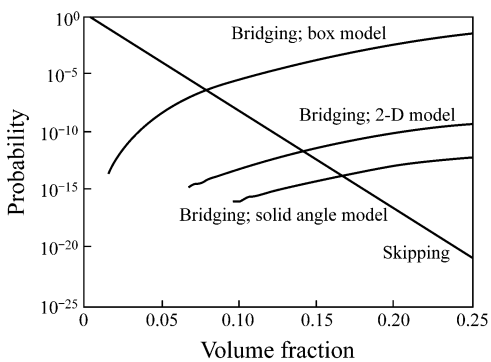

Fig.15 Probability of particles bridging gap as a function of filler volume fraction (Courtesy of S.H. Mannan)

3.2.2 ACA flow during bonding

As modelled by Mannan, *et al.*[18], there are two types of adhesive flow during the ACA bonding (Fig.16). Type I flow occurs around individual pads and bumps at the beginning of bonding, filling voids nearby. After voids are completely filled, type II flow becomes dominant, expelling the adhesive from under the chip to edges.

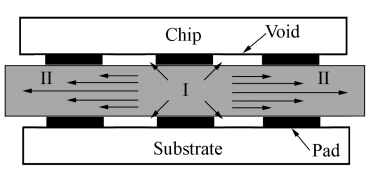

Fig.16 Schematic drawing of the ACA flow during the bonding (Courtesy of S.H. Mannan)

By solving the Navier-Stokes equations of Newtonian fluid, one can obtain the following equation that describes the pressure distribution under the chip in the cylindrical coordinate system:

$$P(r) = \frac{2F}{\pi R^2}\left(1 - \frac{r^2}{R^2}\right), \tag{15}$$

where R is half of the side length of the chip and F is the bonding force. In reality, the ACA resin probably behaves more like power law fluids:

$$\tau_{xy} = \eta_0 \left(\frac{\mathrm{d}\gamma}{\mathrm{d}t}\right)^n, \tag{16}$$

where η_0 is termed as the consistency and n the power law index. For a Newtonian fluid, n equals 1 and η_0 becomes the viscosity of the fluid. As the chip is pressed down, the ACA is squeezed out between the chip and substrate. With power law fluids, the process time t_p for reducing the gap height from h_0 to h_1 is given by

$$t_p = \frac{2n+1}{n+1}\left(\frac{2\pi\eta_0 R^{n+3}}{F(n+3)h_0^{n+1}}\right)^{\frac{1}{n}}\left(\left(\frac{h_0}{h_1}\right)^{\frac{n+1}{n}} - 1\right). \tag{17}$$

This process time is important for determine the suitable heating ramp for bonding. Too high bonding temperature may cause the adhesive solidify before particles are deformed completely, resulting in less reliable joints.

3.2.3 Electrical conduction development and residual stresses

As ACAs contain a small volume fraction of particles, there is no conduction in any direction before bonding. The electrical resistance starts to decrease as pressure increases due to enlarged contact area. Several research groups have reported the deformation effect on the electrical conduction development during the ACA assembly. The first publication is from Williams, *et al.*[19] and the contact resistivity ρ of an ACA joint was estimated as:

$$\rho = \frac{A_{\rho_B}\left(\sqrt{\frac{6\pi nk}{\sigma A}} - \frac{1}{R_B}\right)}{4\pi n R_B}, \tag{18}$$

where ρ_B is the resistivity of the conductive particle, n is the number of contacts within the contact area A, k is the shear yield stress of a conductive particle with a radius of R_B, and σ is the pressure applied to the joint.

With a combination of analytical method and FEM, Hu, *et al.*[20] derived the relationship between the resistance and bonding pressure both for the rigid and deformable particle systems, as shown in Fig.17. They also simulated the contact between the particle and electrode with FEM. As shown in Fig.18, significant compressive stress is found to build up in the interface between the two contacts. This stress is believed to generate peel stress in the adhesive, which is probably the reason for catastrophic failure.

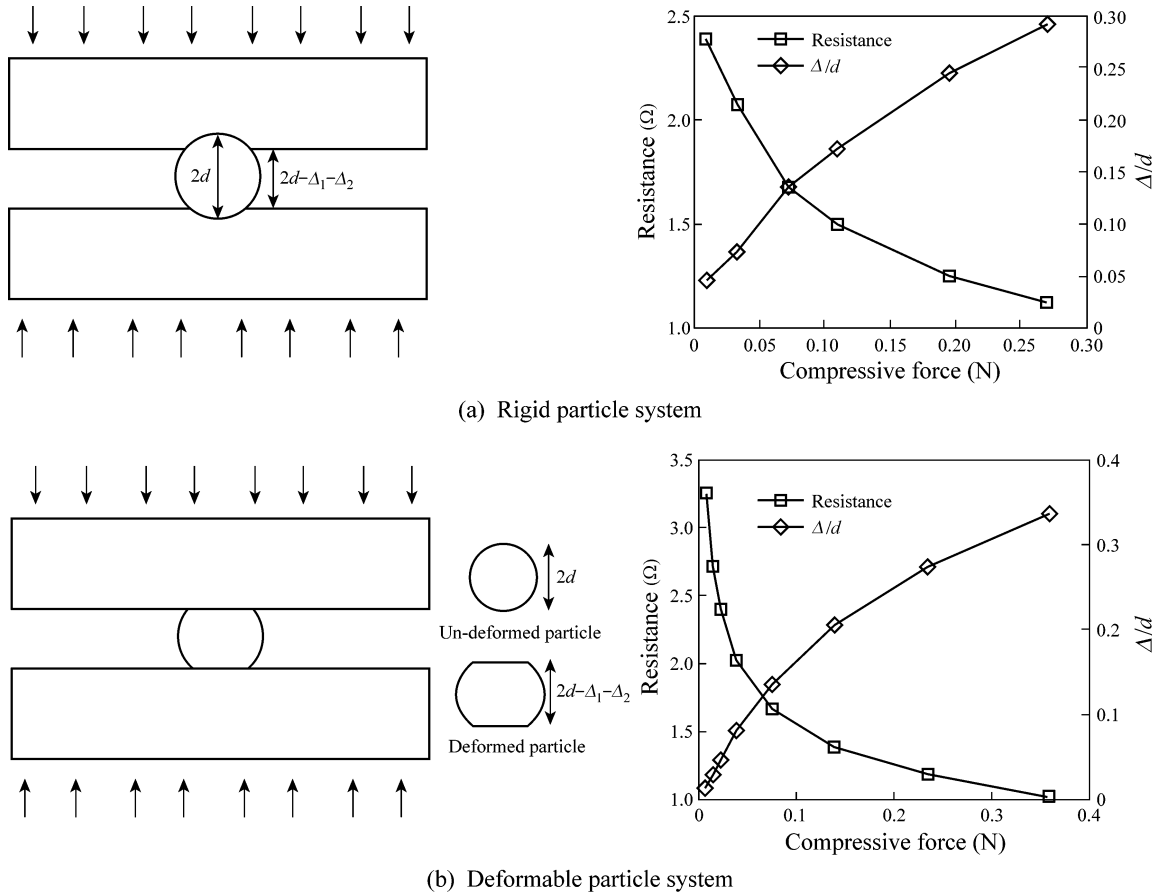

Fig.17 Force-resistance-deformation relationships for rigid particle system and deformable particle system (Courtesy of C.P. Yeh)

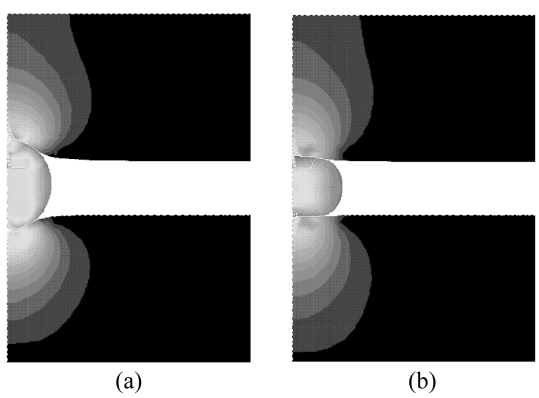

Fig.18 Deformation distributions of (a) rigid particle system and (b) deformable particle system (Courtesy of C.P. Yeh)

Fu, *et al.*[21] considered multi-particle case and found that the particle location in an ACA joint can affect its electric conductance. As shown in Fig.19, a particle in the centre of the joint contributes much more to the electrical performance than a particle close to the edge of the joint. This helps to explain why the measured resistance scatters greatly from one joint to another. Increasing the number of particles on the contact pad can improve the uniformity of the electric conduction. It however also increases the constriction resistances due to fellow particles. So the total conductance does not increase in the additive manner.

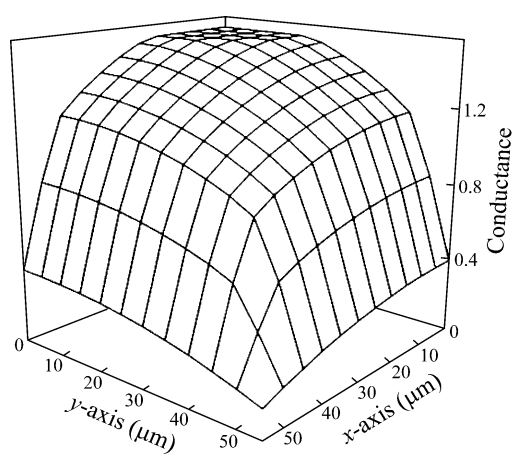

Fig.19 Electric conductance of the particle as a function of its location away from the center of the ACA joint

3.2.4 A generic model for reliability modelling of anisotropic conductive adhesive joints

The traditional 3-parameter Weibull distribution, named after Waloddi Weibull[22] has the following form:

$$F(t) = 1 - \exp\{-[(t-\tau)/\alpha]^{\beta}\}, \quad t \geqslant \tau, \tag{19}$$

where α is the scale parameter, β is the shape parameter which is a kind of wear characteristic or associated with different failure modes, and τ is the location parameter indicating the minimum life.

3.2.4.1 Failure-criteria dependence of the location parameter

Since α and β in the Weibull distribution are material dependent with α characterizing the strength of the material and β characterizing the aging effect of the material, it can be assumed that they are independent of the failure criterion in this case. However, the location parameter τ should depend on the failure criterion because of the cumulative damage leading to a failure. Here we report the 4-parameter Weibull distribution to handle the reliability of the anisotropic conductive adhesives.

Let the failure criterion be generally described as $r > kr_0$, where r_0 is the nominal level. A generalized model can be developed under this framework.

Let τ_0 be the location parameter at the nominal value. Here we assume that this location parameter τ_0 is greater than zero, which means that the material has a failure-free life until τ_0. Some preliminary analysis indicates that a model for τ could be

$$\tau = \tau_0 k^b, \tag{20}$$

where b is an empirical parameter to be estimated with test data. That is, the probability of failure at time t depends on the value of k in the following manner:

$$F(t;k) = 1 - \exp\{-[(t-\tau_0 k^b)/\alpha]^{\beta}\}. \tag{21}$$

Hence this is a model with four parameters, but it can be fitted to the data sets under different criteria at the same time.

Such a model is useful in many aspects. Some are discussed in the following.

First, the minimum life defined as $\tau = \tau_0 k^b$ can be computed for any given failure criteria. This provides a theoretical explanation of the existence of the minimum life and its dependence of the failure criteria. In fact, it is this application that had motivated our study of this approach.

Second, fixing a minimum cycle time to failure, the failure criterion that meets this requirement can be determined. This is useful in contractual situation when a minimum cycle time is to be guaranteed. That is, if the required or guaranteed minimum cycle life is τ_r, from the inequality $\tau_0 k^b \geqslant \tau_r$, we get that $k \geqslant (\tau_r/\tau_0)^{1/b}$. In other words, the failure criteria can at most be set as $k = (\tau_r/\tau_0)$.

Furthermore, under any failure criterion, the cumulative failure probability can be computed at any time. With all the four parameters known or estimated from data collected in several experimental criteria, estimation of the cumulative failure probability at any time under any criterion can be inferred from the above model. Such inference can be useful and convenient for application and further related study.

3.2.4.2 Least square estimation

The general model contains four parameters that have to be estimated using the data from testing. Various methods can be used, and here the parameters can be estimated by simple least square method. Here the cumulative distribution function is estimated by the mean ranking with the form

$$\hat{F}_{ij} = \frac{j}{n_i + 1} \tag{22}$$

and the sum of square deviation can be written as

$$\begin{aligned} \text{SSE} &= \sum_{i=1}^{m}\sum_{j=1}^{d_i}[\hat{F}_{ij}(t) - F_{ij}(t)]^2 \\ &= \sum_{i=1}^{m}\sum_{j=1}^{d_i}\left[1 - \frac{j}{n_i+1} - \exp\{-[(t_{ij} - \tau_0 k_i^b)/\alpha]^{\beta}\}\right]^2, \end{aligned} \tag{23}$$

where m different failure criteria have been considered, and n_i samples are tested for each criterion i, and k_i is the criterion parameter of criterion i. For each sample group with n_i samples, d_i components have failed, and t_{ij} is the time to failure for the j-th failed component.

Since parameter τ_0 is defined as the location parameter at the nominal failure criterion, it is suggested to use the sample data under the nominal failure criterion to estimate the parameter τ_0.

Therefore, the minimization of SSE is accomplished by taking the partial derivatives of SSE with respect to the parameters and setting the resulting equations to zero, which leads to Eqs.(24)–(27):

$$\frac{\partial \text{SSE}}{\partial \alpha} = -2\frac{\beta}{\alpha}\sum_{i=1}^{m}\sum_{j=1}^{d_i}\left[1 - \frac{j}{n_i+1} - \exp\{-[(t_{ij} - \tau_0 k_i^b)/\alpha]^{\beta}\}\right]\exp\{-[(t_{ij} - \tau_0 k_i^b)/\alpha]^{\beta}\}[(t_{ij} - \tau_0 k_i^b)/\alpha]^{\beta} = 0, \tag{24}$$

$$\frac{\partial \mathrm{SSE}}{\partial \beta} = 2\sum_{i=1}^{m}\sum_{j=1}^{d_i}\left[1-\frac{j}{n_i+1}-\exp\{-[(t_{ij}-\tau_0 k_i^b)/\alpha]^\beta\}\right]\exp\{-[(t_{ij}-\tau_0 k_i^b)/\alpha]^\beta\}(t_{ij}-\tau_0 k_i^b)^\beta \ln[(t_{ij}-\tau_0 k_i^b)/\alpha] = 0, \tag{25}$$

$$\frac{\partial \mathrm{SSE}}{\partial b} = -2\tau_0\frac{\beta}{\alpha}\sum_{i=1}^{m}\sum_{j=1}^{d_i}\left[1-\frac{j}{n_i+1}-\exp\{-[(t_{ij}-\tau_0 k_i^b)/\alpha]^\beta\}\right]\exp\{-[(t_{ij}-\tau_0 k_i^b)/\alpha]^\beta\}[(t_{ij}-\tau_0 k_i^b)/\alpha]^{\beta-1}k_i^b \ln k_i = 0, \tag{26}$$

$$\frac{\partial \mathrm{SSE}}{\partial \tau_0} = -2\frac{\beta}{\alpha}\sum_{i=1}^{m}\sum_{j=1}^{d_i}\left[1-\frac{j}{n_i+1}-\exp\{-[(t_{ij}-\tau_0 k_i^b)/\alpha]^\beta\}\right]\exp\{-[(t_{ij}-\tau_0 k_i^b)/\alpha]^\beta\}[(t_{ij}-\tau_0 k_i^b)/\alpha]^{\beta-1}k_i^b = 0. \tag{27}$$

The above equations can be solved using computer spreadsheet or software. Also note that the location parameter model $\tau_i = \tau_0 k_i^b$ should satisfy the condition that $\tau_i \leqslant t_{i1}$ under each failure criterion i.

3.2.4.3 The experiment and data

The general approach above is proposed for the analysis of conductive adhesive joining in flip-chip packaging. This is considered to be one of the important packaging methods as this technology offers potentials for low cost, high reliability and simpler processing. Some of the work on the process optimization, environmental aspects in this novel emerging technology have been published previously by several authors and groups[23−27].

A significant number of accelerated reliability tests under well-controlled conditions is based on single joint resistance measurement to generate significant reliability data for using anisotropic conductive adhesive flip-chip technology on FR-4 substrate. Nine types of anisotropic conductive adhesive (ACA) and one non-conductive film (NCF) were used. In total, nearly one thousand single joints were subjected to reliability tests in terms of temperature cycling between −40 ℃ and 125 ℃ with a dwell time of 15 min and a ramp rate of 110 ℃/min. The test chip used for this extensive reliability test had a pitch of 100 μm. Therefore, the test was particularly focused on evaluation on the reliability of ultra fine pitch flip-chip interconnections using ACA on a low-cost substrate.

The reliability was characterized by single contact resistance measured using the four-probe method during temperature cycling testing up to 3000 cycles. The failure definition is defined as 20% increase, larger than 50 mΩ and larger than 100 mΩ respectively using the *in-situ* electrical resistance measurement technique. Usually when tests are carried out in different conditions or when the data is from different failure criteria, the data sets are analyzed separately. This usually involves a large number of combined model parameters and there is no clear relationship between the model parameters.

The test set-up: To study the reliability of conductive adhesive joints, contact resistance of single joints is one of the most important parameters. Therefore, a test chip was designed for four-probe measurement of single joints. The configuration of the test chip contains 18 single joints and two daisy-chains (18 joints for each). The pitch of the test chips is 100 μm. Bump metallization of the chips is electroless nickel and gold. Table 3 summarizes some characteristic parameters of the test chip. Here, the reliability study focused on the reliability of ACA joining, *i.e.* the characteristics of ACA joints together with the usage environment. A temperature cycling test was applied for the evaluation. The reliability of ACA joints was characterized by the change of contact resistance in the cycled temperatures. A total of 954 joints (53 chips) with different ACA materials were tested. Two chips with 36 joints were measured in situ with the four-probe method during testing up to 3000 cycles, and other joints were taken out from the equipment every several hundred cycles to manually measure the resistance change in room temperature.

Table 3 Technical data of silicon test chips used in this work

Chip size (mm)	Bump (μm)		Pitch (μm)	No. of bumps
	Size	Height		
3.0 × 3.0	60	20	100	54

The test was performed in a temperature cycling cabinet Heraeus Vötsch VMS 3. ACA joints were tested from −40 ℃ to 125 ℃. The dwell time was 15 min and the ramp rate was 110 ℃/min (temperature transition from −40 ℃ to 125 ℃ in 1.5 min).

Most ACA joints were manually measured every several hundred cycles because of the capacity of the cabinet. A total of 918 joints (51 chips) were tested. Some of them, 126 joints of 7 chips, failed after only 200 cycles due to bad alignment, so they were screened out. The remaining 792 joints (44 chips) were tested for 1000 cycles. Cumulative failures of the ACA Flip-Chip joints were measured manually at room temperature, according to different criteria (*i.e.* the resistance increase was over 20%, contact resistance was over 50 mΩ and 100 mΩ).

Test results and discussions: Cumulative fails of the *in-situ* testing are shown in Fig.20. The number of fails is dependent on the definition of the failure. Fig.20 shows three statistics on the cumulative fails respectively based on the different criteria: > 20% of contact resistance increase; > 50 mΩ; > 100 mΩ. When the criterion was defined at 20% of resistance increase, after 2000 cycles all of joints failed. This definition might be too harsh for those joints only having a contact resistance of several mΩ. The 20% increase means only a few milliohm is allowed to vary. In some case, the limitation is still within the margin of error of the measurement.

If we, in any case, allow 50 mΩ or 100 mΩ as the failure criteria, we will obtain a mean time to failure (MTTF) value of 2500 and 3500 cycles respectively from simple Weibull probability plot. Therefore, it is reasonable that the criterion is defined according to the production requirements. Fig.3(a) shows an example of an ACA joint resistance change measured by *in-situ* technique during cycling.

A problem in the analysis of this type of data is that failures under different criteria are usually analyzed separately. With a small number of data points and a large total number of model parameters, the analysis is usually inaccurate. It would be useful to develop an approach for joint analysis of the data sets. The following sections present a Weibull model with the analysis of the data in Fig.3(a) as an example.

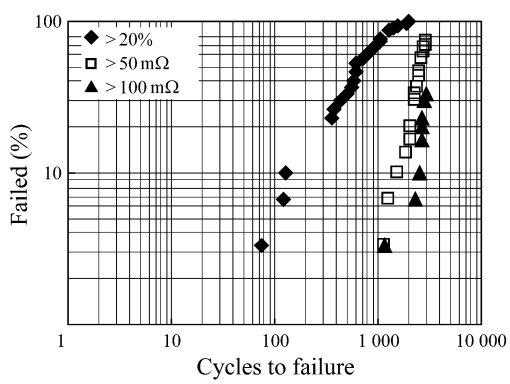

Fig.20 Cumulative failure plot during the temperature cycling test

3.2.4.4 Analysis and the results

Here we will follow the general model presented earlier. Data of the failure of adhesive flip-chip joints on an FR-4 substrate during the temperature cycling test is considered to illustrate the above new model and estimation. Under criterion II (failure if resistance > 50 mΩ), and criterion III (failure if resistance > 100 mΩ), the cumulative number of failures is summarized in Table 4. The nominal level of the test (r_0) is 6 mΩ, thus the criterion parameters k_1 and k_2 are $r_1/r_0 = 50/6 = 8.33$, r_2/r_0=100/6=16.67, respectively. Using simple spreadsheet, the traditional least square estimation of the parameters is given by

$$\alpha = 1954, \quad \beta = 4.076, \quad \tau_0 = 370,$$
$$b = 0.409 \text{ and SSE} = 0.1261.$$

The overall model is then given by

$$F(t;k) = 1 - \exp\{-[(t - 370k^{0.409})/1954]^{4.076}\}, \qquad (28)$$

where k is the failure criterion in terms of 'failure when the resistance is k times of the nominal value'. This above formula can be used for different failure criteria.

Table 4 Cumulative number of failures under different criteria

Cycles to failure	Cumulative number of failures	
	Criterion II (>50 mΩ)	Criterion III (>100 mΩ)
1170	1	1
1300	2	-
1550	3	-
1925	4	-
2050	5	-
2100	6	-
2300	9	2
2350	10	-
2400	11	-
2500	13	3
2550	14	-
2600	-	5
2650	17	6
2700	-	7
2750	-	9
2800	19	-
2850	20	-
2900	21	-
2950	22	10

3.2.4.5 Application of the results

From the above analysis, note that the minimum cycle life is given by

$$\text{Minimum life} = 370k^{0.409}.$$

Hence, for any given failure criterion, we can obtain the minimum life with this formula. The estimated minimum life at failure definition of larger than 50 mΩ and larger than 100 mΩ are 880.68 and 1169.33, respectively. Table 5 shows the estimated minimum life and MTTF under some different failure conditions.

Furthermore, for fixed or agreed cycle to failure, we can obtain the maximum failure criteria as

$$370k_0^{0.409} > c_0, \text{that is } k_0 > \left(\frac{c_0}{370}\right)^{1/0.409}.$$

That is, to be sure that the minimum life is c_0, the failure criteria cannot be more stringent than 'failure when the resistance is k_0 times of the nominal value'. This is, for example, a statement that can be used together with the minimum life requirement, and can be added in the contractual situation.

Table 5 Minimum life (c_0) and MTTF under different failure criteria (cycle)

K_0	c_0	MTTF
1	370.00	2143.08
2	491.34	2264.42
3	580.02	2353.10
4	652.48	2425.56
5	714.86	2487.94
6	770.23	2543.32
7	820.39	2593.49
8	866.46	2639.54
9	909.24	2682.33
10	949.30	2722.38
20	1260.63	3033.71
30	1488.14	3261.22
40	1674.05	3447.13
50	1834.11	3607.19

4 Conclusion

Anisotropic conductive adhesive interconnection for low-cost flip-chip and surface mount applications is an emerging technology. It has been shown in this overview paper that anisotropic conductive adhesives play a significant role in electronics packaging and are expected to do so for years to come. It is clear that the wider use of adhesives has been recognized in recent decades. An increasing amount of performance data has been generated by research efforts worldwide. More products based on adhesive joining technology are appearing, especially in the field of flip-chip assembly. However, further reliability data and real service life prediction tools are necessary for this environmentally friendly and low-cost technology to be fully accepted.

Acknowledgment

The authors wish to thank their colleagues: LAI Zong-he, FU Ying, CHEN Liu, CHENG Zhao-nian, MO Zhi-min and ZOU Gang, who have been engaged in conductive adhesive research at Chalmers and have generated a tremendous research results during last ten years. Also we wish to acknowledge the financial support from the SMIT Center member company: Hitachi Chemicals, Japan.

References

[1] Gilleo K. Assembly with conductive adhesives[J]. *Soldering and Surface Mount Technology*, 1995, (19): 12–17.

[2] Chang D D, Crawford P A, Fulton J A, Mcbride R, Schmidt M B, Sinitskir E, Wong C P. An overview and evaluation of anisotropically conductive adhesive films for fine-pitch electronic assembly[J]. *IEEE Transactions on Components Hybrids and Manufacturing Technology*, 1993, **16**(8): 828–835.

[3] Savolainen P, Kivilahti J. A solder alloy filled *Z*-axis conductive epoxy adhesive[J]. *Journal of Adhesion*, 1995, **49**(3–4): 187–196.

[4] Kristiansen H, Liu J. Overview of conductive adhesive interconnection technologies for LCD's[J]. *IEEE Transactions on Components Packaging and Manufacturing Technology Part A*, 1998, **21**(2): 208–214.

[5] Liu J, Lai Z. Reliability of anisotropically conductive adhesive joints on a flip-chip/FR4 substrate[J]. *Journal of Electronic Packaging*, 2002, **124**(3): 240–245.

[6] Lai Z, Liu J. Anisotropically conductive adhesive flip-chip bonding on rigid and flexible printed circuit substrates[J]. *IEEE Transactions on Components Packaging and Manufacturing Technology Part B*, 1996, **19**(3): 644–660.

[7] Yim M J, Paik K W. Design and understanding of anisotropic conductive films (ACF's) for LCD packaging[J]. *IEEE Transactions on Components Packaging and Manufacturing Technology Part A*, 1998, **21**(2): 226–234.

[8] Chan Y C, Luk D Y. Effects of bonding parameters on the reliability performance of anisotropic conductive adhesive interconnects for flip-chip-on-flex packages assembly I. Different bonding temperature[J]. *Microelectronics Reliability*, 2002, **42**: 1185–1194.

[9] Tan S C, Chan Y C, Chin Y W, Tan C W. Thermal stability performance of anisotropic conductive film at different bonding temperatures[J]. *Microelectronics Reliability*, 2004, **44**: 495–503.

[10] Yin C Y, Alam M O, Chan Y C, Bailey C, Lu H. The effect of reflow process on the contact resistance and reliability of anisotropic conductive film interconnection for flip chip on flex applications[J]. *Microelectronics Reliability*, 2003, **43**(4): 625–633.

[11] Seppälä A, Ristolainen E. Study of adhesive flip chip bonding process and failure mechanisms of ACA joints[J]. *Microelectronics Reliability*, 2004, **44**(4): 639–648.

[12] Liu J, Tolvgard A, Malmodin J, Lai Z. A reliable and environmentally friendly packaging technology—flip-chip joining using anisotropically conductive adhesive[J]. *IEEE Transactions on Components and Packaging Technologies*, 1999, **22**(2): 186–190.

[13] Lai Zong-he, Lai Ruo-yin, Persson K, Liu J. Effect of bump height on the reliability of ACA flip chip joining with FR4 rigid and polyimide flexible substrate[J]. *Journal of Electronics Manufacturing*, 1998, **8**(3–4): 217–224.

[14] Khoo C G L, Liu J. Moisture sorption in some popular conductive adhesives[J]. *Circuit World*, 1996, **22**(4): 9–15.

[15] Liu J. On the failure mechanism of anisotropically conductive adhesive joints on copper metallisation[J]. *International Journal of Adhesion and Adhesives*, 1996, **16**(4): 285–287.

[16] Mo Zhi-min, Lai Zong-he, Li Shi-ming, Liu J. Thermal fatigue cracking of surface mount conductive adhesive joints[J]. *Soldering and Surface Mount Technology*, 2004, **16**(1): 48–52.

[17] Mannan S H, Williams D J, Whalley D C. Some optimum processing properties for anisotropic conductive adhesives for flip chip interconnection[J]. *Journal of Materials Science—Materials in Electronics*, 1997, **8**(4): 223–231.

[18] Mannan S H, Williams D J, Whalley D C, Ogunjimi A O. Models to determine guidelines for the anisotropic conducting adhesives joining process[C]// Liu J, ed. *Conductive Adhesives for Electronics Packaging*, Port Erin, Isle of Man, UK: Electrochemical Publications Ltd, 1999, 78–98.

[19] Williams D J, Whalley D C, Boyle O A, Ogunjimi A O. Anisotropic conducting adhesives for electronic interconnection[J]. *Soldering and Surface Mount Technology*, 1993, (14): 4–8.

[20] Hu K X, Yeh C P, Wyatt K W. Electro-thermo-mechanical responses of conductive adhesive materials[J]. *IEEE Transactions on Components Packaging and Manufacturing Technology Part A*, 1997, **20**(4): 470–477.

[21] Fu Y, Willander M, Liu J. Statistics of electric conductance through anisotropically conductive adhesive[J]. *IEEE Transactions on Components and Packaging Technologies*, 2001, **24**(2): 250–255.

[22] Lai Z, Liu J. Anisotropically conductive adhesive flip-chip bonding on rigid and flexible printed circuit substrates[J]. *IEEE Transactions on CPMT, Part B: Advanced Packaging*, 1996, **19**(3): 644–660.

[23] Joyce C F. A Weibull model to characterize lifetimes of aluminum alloy electrical wire connections[J]. *IEEE Transactions on CPMT*, 1991, **14**(1): 124–133.

[24] Gerke R D, Kromann G B. Solder joint reliability of high I/O ceramic-ball-grid arrays and ceramic quad-flat-packs in computer environments: The PowerPC 603 (TM) and PowerPC 604 (TM) microprocessors[J]. *Solder Joint Reliability of High I/O Ceramic-Ball*, 1999, **22**(4): 488–496.

[25] Pecht M G, Shukla A A, Kelkar N, Pecht J. Criteria for the assessment of reliability models[J]. *IEEE Transactions on CPMT, Part B: Advanced Packaging*, 1997, **20**(3): 229–234.

[26] Tamai T. Effect of silicone vapor and humidity on contact reliability of micro relay contacts[J]. *IEEE Transactions on CPMT, Part A: Packaging Technologies*, 1996, **19**(3): 329–338.

[27] Weibull W. A statistical distribution function of wide applicability[J]. *Journal of Applied Mechanics*, 1951, **18**(3): 293–296.

(*Editor WANG Hai-jiang*)